None-Line-Of-Sight Imaging Beyond The Corner

Xisen Wang[1] and Ge Jin[2]

[1] Beijing 21st Century International School xisen.wang@keble.ox.ac.uk
[2] The Affiliated High School of Peking University gejin@berkeley.edu

Abstract. With various applications in robotics, autonomous vehicles, and medical imaging, none-line-of-sight(NLOS) imaging involves the reconstruction of an object hidden from view. Compared to most research that only examines third-order bounces of indirect illuminations, this paper investigates the five-bounce NLOS imaging problem by proposing a new algorithm derived from the Huygens–Fresnel principle, Light Cone Transform (LCT), and light field migration. The paper first presents a mathematical model for five-bounce imaging and then, from the model, derives the five-bounce algorithm. Various transformations are made to convert the algorithm into a computationally efficient methodology, with four sub-algorithms presented in the Supplement Document. In the end, the five-bounce algorithm is applied to three simulated scenes with a confocal scanning approach, producing high-quality reconstructions.

Keywords: Confocal non-line-of-sight imaging · Light cone transform · Diffuse reflection · Huygens–Fresnel principle · computational photography

1 Introduction

In recent years, there has been significant research on non-line-of-sight (NLOS) imaging. Unlike conventional LOS imaging (Sun et al, 2013, Shin et al.2016), which calculates the time taken by a light pulse to move along a direct path, NLOS imaging employs multi-bounce light paths to indirectly determine the 3D form of concealed objects (Kirmani et al. 2009; Velten et al., 2012). This technique generally utilizes the data encoded in the time-of-flight of dispersed photons. With the ability to "see" objects hidden from direct paths of sight, NLOS imaging is essential in many fields, including robotic vision, medical imaging, search and rescue, remote sensing, and etc.

Much progress has been made, and we wish to dedicate the Related Work Section to describe a general development outline. Most work share the same assumption that there is only one surface of occlusion and consequently three bounces of diffuse reflections. However, in most realistic scenarios, there would be at least two occlusion surfaces, and light is propagated with five bounces of diffuse reflection. Hence, a method that targets five and higher order bounces of indirect illumination is needed to extend the application of NLOS Imaging to more complex scenarios.

To solve the above problem, we present a five and higher order bounce NLOS imaging approach that reconstructs an image from more than one corner, expanding the applicability of NLOS imaging in different scenarios. By using retroreflective materials and setting other assumptions, we simplify the problem into calculating two distances. We build our work upon the great progress of LCT and fast f-k migration methods, which will be illustrated in the Related Work Section. By using confocal scanning approach to set the problem layout as LCT does, and express the confocal NLOS image formation with wave equation, we interpret the reconstruction problem as a boundary value problem. Different to existing work that only consider one stage of light propagation with two boundaries, we consider the light transport problem with two stages, namely bouncing from the first occlusion and then the second. Our proposed algorithm is demonstrated to reconstruct image with good quality, as shown in our MATLAB simulation in later sections.

As the research remains mostly theoretical, we suggest time-resolved detectors such as single-photon avalanche diodes (SPAD) for experimental verification in the future. Our algorithm has demonstrated the potential of five-order NLOS imaging for extending the applicability of NLOS imaging, so various explorations could be built on our methods to investigate the problem further. Our approach and interpretation of five-bounce NLOS Imaging problem, with mathematical simplification and computational implementation, pave the way for the research community to dive into NLOS problems that are more intricate and involve more corners.

2 Related Work

2.1 General Overview

Non-line-of-sight (NLOS) imaging, which aims to reconstruct the shape and albedo of hidden objects from multiply scattered light, has garnered significant attention from the research community since its introduction by Kirmani in 2009. Velten (2009) developed this concept further and discussed the challenge of recovering obscured objects in imaging. He presented a new approach that uses a combination of time-of-flight technique and computational reconstruction algorithms to untangle mixed image information caused by diffuse reflection. However, this method has limitations such as low speed, restrictive assumptions, and the nature of approximation.

To address these problems, researchers have proposed various solutions, investigating different angles and methods. There has been significant progress in transient imaging techniques (Jarabo et al., 2017) that use gated sensors (Laurenzis et al., 2014), streak cameras (Velten et al., 2013), amplitude modulated continuous waves (Gupta et al., 2015), single-photon avalanche diodes (O'Toole, 2017), and interferometry (Gkioulekas, 2015). Additionally, optical techniques for NLOS imaging include speckle correlations (O Katz, 2014), acoustic echoes (Dokmanic, 2013), confocal imaging (O'Toole, 2018), intensity imaging (Klein,

2016), among others.Passive approaches to NLOS imaging have also been explored (Baradad et al., 2018; Boger-Lombard and Katz, 2018; Bouman et al., 2017; Saunders et al., 2019). However, most of these approaches are limited by strong assumptions of light transport, restricted application to microscopic settings, and insufficient information about the hidden scene.

Researchers kept innovating upon the algorithm to tackle the NLOS problem. Several important examples are examined here. Gariepy (2016) attempted to reduce NLOS imaging to a simpler tracking problem, while Pediredla (2017) used a parametric planar model to represent the hidden scene. O'Toole (2018) proposed the Light-Cone-Transform (LCT) approach that generates quality image reconstruction while relies on retroreflective materials and confocal scanning. Tasi et al. (2019) analyzed the geometry of specular paths by solving an inverse rendering problem. Besides, Liu et al. (2019) demonstrated NLOS imaging of complicated scans with strong multiple scattering and arbitrary materials, by phasor-field virtual wave optics approach. Meanwhile, Lindell et al. (2019) explored wave-based NLOS imaging using fast f-k migration to provide quality image reconstruction while loosening many assumptions and restrictions. These methods, however, focus primarily on NLOS imaging across only one corner, and thus assumes only three bounces of indirect illumination.

Regarding experiments, some researchers have chosen to use alternative sensing technologies, such as photonic mixer devices (PMDs), which are implemented in time-of-flight cameras (Heide et al. 2014), or even conventional camera sensors (Klein et al. 2016; Saunders et al. 2019). Nonetheless, many researchers have favored the use of single-photon avalanche diodes (SPADs) for non-line-of-sight (NLOS) imaging (Buttafava et al., 2015; Xu et al. 2018; Liu et al., 2019). These sensors have the ability to detect the precise arrival time of individual photons within a temporal accuracy of tens of picoseconds. SPADs are also quite versatile, facilitating NLOS imaging at considerable distances, in ambient lighting, and at high speeds (Chan et al. 2017; O'Toole et al., 2018). Xu (2015) proposed a depth and reflectivity imaging system based on SPAD. The detector array with coarsely time-binned photon detector was utilized to reconstruct a scene's 3D structure. In 2021, Wu et al. accomplished NLOS imaging over 1.43 km by developing a fully integrated InGaAs/InP negative-feedback SPAD. Regarding the promising nature of SPAD, we recommend the use of SPAD for experiment validation of our algorithm.

2.2 Light Cone Transform and Fast f-k migration

Among all the methods elaborated above, two methods are of our most interest. They are the Light-Cone-Transform method (O'Toole, 2018) and fast f-k migration method (Lindell, 2019).

O'Toole (2018) introduced a new approach to NLOS imaging reconstruction based on confocal scanning, which has several advantages over previous methods. This approach enables the derivation of the LCT and provides a closed-form solution, reducing the computational and memory requirements for NLOS imaging. LCT makes assumptions such as single scattering behind the wall, isotropic

scattering, and no occlusions within the hidden scene. It treats the problem of NLOS imaging as a spatially invariant 3D deconvolution problem, where the solution involves representing the LCT as a 3D convolution between the vectorized measurements and the vectorized volume of the albedos of the hidden surface, which can be efficiently computed in the Fourier domain.

However, the LCT method is limited in its ability to handle non-planar sampling and non-confocal scanning methods. Lindell (2019) proposed the f-k migration method, a frequency-domain approach, to address the potential drawbacks in the LCT method. The f-k migration method is robust to complex reflectance properties, faster, and more memory-efficient than the LCT method, producing higher quality reconstructions. This method transforms time-domain signals into the frequency domain using a Fourier transform to solve the inverse scattering problem. In particular, it focuses on the boundary conditions and describes the light transport process as wave migration.

Our five-bounce method builds upon the LCT and f-k migration methods, which have primarily focused on the third-order bouncing problem. We adopt these two methods in different stages of the light transport process and hence develop techniques to address higher-order bouncing problems. Our research is crucial to unlocking the full potential of NLOS imaging in various applications, including exploring the intricate intestines, carrying out more complicated rescue tasks, and avoiding more traffic incidents.

3 Forward Model

3.1 Model Description

The five-bounce indirect illumination problem is modeled as the chart below. A typical model includes two walls of reflection, namely $Wall_A$ and $Wall_B$. The object is positioned in a way that the light from the camera can only reach it with at least five bounces of indirect illumination.

3.2 Assumption and Model Simplification

By using confocal scanning and imaging approach, a light source and a single detector and co-axial, enabling one illuminates 2D points on the visible surface while acquiring time-resolved measurements at the same points instead of exhaustively scanning different combinations of light source positions and detector positions on the wall. With this set-up, light propagates to the hidden scene only along very specific paths. The light source sends laser light to Point B on Wall B, which could be considered a virtual signal-transmitter. Five-bounce path starts from light reflected from Wall B to Wall A (BA), from Wall A to the object (AO), from the object back to Wall A (AO), from Wall A back to Wall B (AB), from Wall B back to the detector (BD).

With five and higher-order bounce indirection illumination, the signal is very weak. In order to generate a signal strong enough to carry out experiments

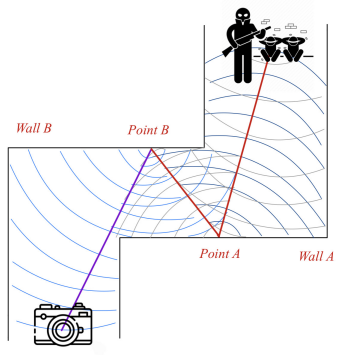

Fig. 1: A schematic diagram of a confocal scanning and imaging approach used for non-line-of-sight imaging with five bounces of diffuse reflections. The set-up enables the acquisition of time-resolved measurements at specific points on the visible surface, eliminating the need for exhaustive scanning of different light source and detector positions.

(needed revision), retroreflective materials are used. Given that retroreflective materials (RRMs) reflect incoming radiation back toward its source of origin (Wang et al., 2021), AO and OA are essentially same pathways. With the suitable adjustment, the light source (camera) could be in the same position as the detector. Hence, both the signal transmission and reception focus at Point A, setting AB equal to BA. Provided that the distance from the light source to Point A needs little consideration, the focus of the problem becomes the estimation of two distances: AB and AO, both of which are the result of indirect illuminations.

3.3 Math Model

This paper adopts two typical assumptions for NLOS-research:

- Light scatters isotropically (so that the model ignores Lambert's cosine terms when modelling diffuse surface reflection).
- No partial occlusions occur within the hidden scene.
- Wall A is in parallel with Wall B

The usual assumption that there is no multi-bounce in light transmission is not required.

3.4 Model Setup

Reflective material properties enable us to calculate the two distances by considering that light is emitted from the object to plane A then to plane B.

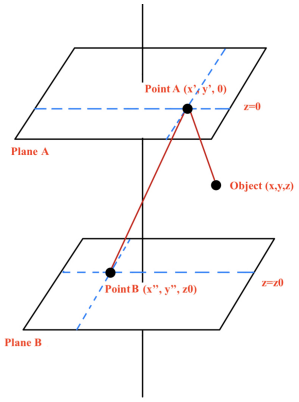

Fig. 2: Five-bounce confocal-NLOS imaging model: the light field at Object O is ρ. The light field at point A is ρ'. The light field at point B is ρ''. Plane A and Plane B are the two occlusion surfaces.

Coordinate Description

The model considers Point A on Plane A, with coordinates $(x', y', 0)$, Point B on Plane B, with coordinates (x'', y'', z_0). To calculate the overall distance travelled by the light, we have $S = OA + AB$, using the general distance Equation:

$$||\vec{r}|| = \sqrt{((x' - x)^2 + (y' - y)^2 + (z' - z)^2)} = 2ct \tag{1}$$

.

Hence, if we later discretize the wall surface into grids of 64*64, then there would be 64^4 (including repeated) pathways to achieve Sum.

Following O'Toole et al.(2018), we interpret the hidden scene as a 3D volume where each voxel emits a spherical wave at t = 0. Following Lindell (2019), we estimate this scene by migrating the field from the first boundary condition (i.e. $z = z, t = 0$), to second boundary condition (i.e. $z = 0, t = t'$), to third boundary condition (i.e. $z = z_0, t = t''$).

From O to A Following Lindell, D.B. et al.[2019], we develop the constraint of wave propagation in space and time by

$$(\nabla^2 - \frac{1}{v^2}\frac{\partial^2}{\partial t^2})\rho = \nabla^2\rho - \frac{1}{v^2}\frac{\partial^2\rho}{\partial t^2} \tag{2}$$

where the Laplacian operator is defined over the spatial dimensions.

According to the Huygens-Fresnel principle, any point on a wave front of sound in a transmitting medium, or light in a transparent medium or vacuum, can be considered as a source of wavelets that propagate in all directions at a speed determined by their respective velocities. Hence, we describe the migration

process from boundary condition at Point O to boundary condition at Point A in the confocal context as:

$$\begin{aligned}\rho'(x', y', t', z' = 0) = \iiint_{\Omega} \frac{1}{r^4}\rho(x, y, z, t = 0) \\ \delta(2\sqrt{(x'-x)^2 + (y'-y)^2 + (0-z)^2} - (t'-t)c)dx\, dy\, dz\end{aligned} \tag{3}$$

In (3), c is the speed of light and $\frac{1}{r^4}$ represents radiometric falloff. Here, function $\rho(x, y, z, t)$ represents the light intensity at (x, y, z) in time t relative to the incident pulse scattered, and function ρ' is with the other boundary condition. The convolution kernel is the surface of a spatio-temporal 4D hypercone given by the distance function. The Dirac Delta function represents the geometric function of light propagation through time and space.

We consider the following Dirac Delta identity from LCT:

$$\int_{\Omega} f(x)\delta(2||x' - x||_2 - tc)dx = \int_{\Omega} f(x)||x' - x||_2\delta(||x' - x||_2^2 - \frac{tc}{2}^2)dx \tag{4}$$

Since the distance function r and the measured time of flight are directly related as below:

$$\frac{2}{c}\sqrt{(x'-x)^2 + (y'-y)^2 + z^2} = t \Leftrightarrow r = \frac{tc}{2} \tag{5}$$

We can pull out the radiometric term from the integral. Combining with the Dirac Delta identity, we rewrite the equation to become:

$$\begin{aligned}\rho'(x', y', t', z' = 0) = \iiint_{\Omega} \frac{1}{r^3}\rho(x, y, z, t = 0) \\ \delta((x'-x)^2 + (y'-y)^2 + z^2 - (\frac{(t'-t)c^2}{2})^2 dx\, dy\, xz\end{aligned} \tag{6}$$

From A to B We consider the same process for the path of light wave from point A to point B, with initial boundary condition $(x', y', z = 0, t')$ and final boundary condition (x'', y'', z_0, t''). Hence we have:

$$\begin{aligned}\rho''(x'', y'', t'', z'' = z_0)) = \iiint_{\Omega} \frac{1}{r^3}\rho'(x', y', t', z' = 0) \\ \delta((x''-x')^2 + (y''-y')^2 + z_0^2 - (\frac{(t''-t')c^2}{2}))dx\, dy\, dz\end{aligned} \tag{7}$$

Our detector and initial signal transmitter are co-located at point B. The whole process results in a two-dimensional collection of temporal histograms. Every measurement sample $\tau(x'', y'', t'')$ could be retrieved from the ρ'' in the relationship as $\tau = Possion(\rho'')$.

Note that since retroreflective materials are utilized, the radiometric falloff term $\frac{1}{r^4}$ in the modeling can be substituted with $\frac{1}{r^2}$. This change indicates a significant enhancement in the indirect light signal as the distance (r) increases.

4 Reconstruction Approach and Algorithm

4.1 Model Adjustment using LCT

We first perform a second change of variable by letting $z = \sqrt{u}$ and $dz/du = 1/2\sqrt{u}$ such that $\rho'(x', y', t) =$

$$(\frac{2}{tc})^3 \iiint_{\Omega} \frac{1}{2\sqrt{u}} \rho(x, y, \sqrt{u}) \delta((x' - x)^2 + (y' - y)^2 + u - v))\, dx\, dy\, dz \tag{8}$$

Then, we introduce a second change of variable using:

$$v = (\frac{(t' - t)c}{2})^2 \tag{9}$$

With:

$$h(x' - x, y' - y, v - u) = \delta((x' - x)^2 + (y' - y)^2 + u - v) \tag{10}$$

such that if we encapsulate important components as:

$$R_t\{\rho'\}(x', y', v) = v^{\frac{2}{3}} \rho'(x', y', \frac{2}{c}\sqrt{v}) \tag{11}$$

$$R_z\{\rho\}(x, y, u) = \frac{1}{2\sqrt{u}} \rho(x, y, \sqrt{u}) \tag{12}$$

We will arrive at the following relationship:

$$R_t\{\rho'\} = h * R_z\{\rho\} \tag{13}$$

For the second step, a similar process is carried out. However, we don't need to change variable to u and v again. Hence, we end up with

$$\rho'' = h' * \rho' \tag{14}$$

The notion * is for convolution. Note here since we input different arguments in calculating the convolution kernel, the kernel is updated. Equation (14) completes the five-bounce image formation model.

4.2 Model Discretization

Forward Bounce In practice, we apply the continuous model above with discrete operations. The discrete Light Cone Transform method is used. The operation in an integral transform could be represented in discrete forms by a matrix-vector multiplication representation of the light intensity ρ' and matrix R_t, and the formula is $R_t\rho'$.

Similarly, a uniform discretion is applied for R_z and ρ so that the corresponding discrete analog of the transformation is defined as matrix-vector multiplication $R_z * \rho$.

With A referring to the light transport matrix, the full discrete image formation model is therefore:

$$\rho' = \mathbf{A}\rho = \mathbf{R_t^{-1}} \mathbf{H} \mathbf{R_z} \rho \tag{15}$$

$$\rho'' = \mathbf{A}'\rho' = \mathbf{H}'\rho' \tag{16}$$

Here, each matrix is applied independently to the respective dimension, enhancing memory efficiency. $\mathbf{H}$ is the discrete version of the kernel h in equation 13, modeling the light transport and migration process. Note that in the second forward bounce, there is not point in transforming and resampling the coordinate with u and v and hence $\mathbf{R_t}$ and $\mathbf{R_z}$ are not used. The efficiency of computation is often improved by using the convolution theorem to perform matrix-vector multiplication with a convolution matrix H as element-wise multiplications in the Fourier domain. Additionally, the inverse of matrix-vector multiplications can be computed using element-wise divisions in the Fourier domain in some cases.

Reconstruction Approach Adopting Otoole (2018)'s assumption for the noise model associated with discrete LCT,

$$\mathbf{R_t}\rho' = \mathbf{H} * \mathbf{R_z}\rho + \eta \tag{17}$$

$$\rho'' = \mathbf{H} * \rho' + \eta \tag{18}$$

Using the Wiener deconvolution filter, we come up with a solution that minimizes the mean square error with respect to the ground truth solution.

$$\rho'_* = \mathbf{F^{-1}} \left[\frac{1}{\hat{\mathbf{H}}} \frac{|\hat{\mathbf{H}}|^{\mathbf{2}}}{|\hat{\mathbf{H}}|^{\mathbf{2}} + \frac{1}{\beta}} \right] \mathbf{F}\rho'' \tag{19}$$

$$\rho_* = \mathbf{R_z^{-1}} \mathbf{F^{-1}} \left[\frac{1}{\hat{\mathbf{H}}} \frac{|\hat{\mathbf{H}}|^{\mathbf{2}}}{|\hat{\mathbf{H}}|^{\mathbf{2}} + \frac{1}{\beta}} \right] \mathbf{F} \mathbf{R_t} \rho' \tag{20}$$

Here, ρ'_* is the light intensity calculated the first back-migration process, and ρ_* is the light intensity calculated for the original object. Matrix $\mathbf{F}$ and $\mathbf{F}'$ represents the 3D discrete Fourier transform. $\hat{H}$ is diagonal matrix containing the Fourier transform of the 3D convolution kernels (i.e. fpsf in implementation), and β is a frequency-dependent term for the signal-to-noise ratio (SNR).

Reconstruction Algorithm In the implementation, we simulate or gain the light intensity at Point B through conversion from the measurements. The whole process has three main steps:

- 1) Get ρ'' from simulation or from measurements. Note that the measurement is the Poisson distribution of light field ρ'' when using a single photon detector.

– 2) reconstruct from point B to point A by (19)
– 3) reconstruct from point A to point B by (20)

$$h(x'-x, y'-y, v-u) = \delta((x'-x)^2 + (y'-y)^2 + u - v) \tag{21}$$

$$h'(x''-x', y''-y', z_0, t''-t) = \delta((x''-x')^2 + (y''-y')^2 + z_0^2) - \frac{(t''-t')c}{2}) \tag{22}$$

The two shift-invariant 3D Convolution kernels are computed using equations (21) and (22). Fourier Transform is then applied to the two kernels.

We refer to a pseudo-code Core Algorithm that describes the five-bounce NLOS imaging reconstruction process. More specific steps are referred to in the Supplemental document.

Algorithm 1 Core Algorithm: Five-Bounce NLOS-Imaging

Begin Procedure
// 1. Get ρ'' from measurement or simulation
Me $\rightarrow$ $PoissonDistribution(\rho'')$ % Measurement Me
// 2. Set the space dimension M, time dimension N, signal-to-noise ratio
$M \leftarrow M_0, N \leftarrow N_0, \beta \leftarrow \beta_0$
// 3. Define shift-invariant convolution kernel from Point B to Point A
$h'(x''-x', y''-y', z_0, t''-t) = \delta((x''-x')^2 + (y''-y')^2 + z_0^2) - \frac{(t''-t')c}{2})$
// 4. Apply Fast Fourier Transform (fftn) on the kernel
$\hat{H}$ = fftn(H)
// 5. Compute the first reconstruction
$\rho'_* = \mathbf{F^{-1}} \left[\frac{1}{\hat{\mathbf{H}}} \frac{|\hat{\mathbf{H}}|^2}{|\hat{\mathbf{H}}|^2 + \frac{1}{\beta}} \right] \mathbf{F}\rho''$
// 6. Compute the second kernel from point A to point O
$h(x'-x, y'-y, v-u) = \delta((x'-x)^2 + (y'-y)^2 + u - v)$
// 7. Compute R_{t-1} and R_z
$R_t\{\rho'\}(x', y', v) = v^{\frac{2}{3}} \tau(x', y', \frac{2}{c}\sqrt{v})$
$R_{t-1} = inv(R_t)$
$R_z\{\rho\}(x, y, u) = \frac{1}{2\sqrt{u}} \rho(x, y, \sqrt{u})$
// 8. Compute the second reconstruction
$\rho_* = \mathbf{R_z^{-1} F^{-1}} \left[\frac{1}{\hat{\mathbf{H}}} \frac{|\hat{\mathbf{H}}|^2}{|\hat{\mathbf{H}}|^2 + \frac{1}{\beta}} \right] \mathbf{F R_t} \rho'$
End Procedure

5 Simulation Experiment

5.1 Scene Setup

In our simulation, we set the space dimension **N** to 128, time dimension **M** to 512, wall size to 2 meteres, bin resolution to $32 * 10^{-12}$, c to $3 * 10^8$ (speed of light) and width to wall size / 2.

We establish three scenes for simulation, with the data format (x, y, z):

– Scene 1: A single dot at (64,64,64)
– Scene 2: A famous statue, from (Lindell et al, 2019)

The simulation method mainly consists of two forward-bounce simulations from the original data (the original shape of the object in each scene). The first step is to calculate the convolution kernel and apply equation 15, and the second step would be to apply equation 16, ending up with ρ'' that could be converted to measurements using certain relations.

5.2 Simulation Result

We construct our simulated measurement using the method derived in the Forward Bounce section in Model Discretization. Applying the proposed algorithm, we came up with following results:

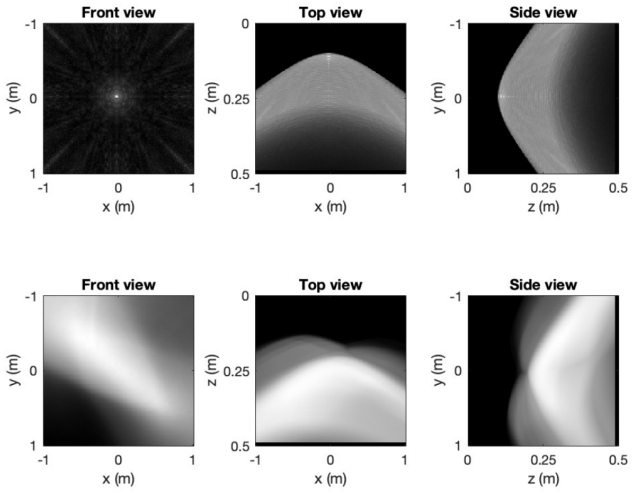

Fig. 3: Simulation of Measurement ρ'': we simulate the measurement of the intensity of light detected at different objects and detector positions.
The simulated measurement consists of three scenes. Scene 1 (Row 1) contains a single dot located at the coordinates. Scene 2 (Row 2) consists of a statue.

For Scene 1, the algorithm took $5.985 + 4.418 = 10.404$ seconds to reconstruct the point. For Scene 2, the algorithm took $6.648 + 12.427 = 19.075$ seconds to

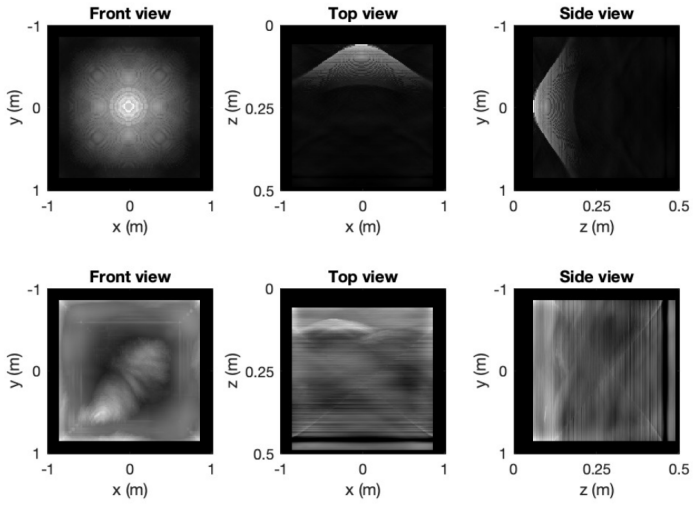

Fig. 4: Reconstruction from B to A: It represents ρ' for three scenes. The reconstruction on the mid-point of the light path. The image appears to be slightly blurry, which can be attributed to the radiometric falloff of light propagation.

reconstruct the shape and volume. The single point is reconstructed with remarkable quality. Although the diffuse statue appears overall dimmer, our algorithm still reconstructs the essential features of this statue with high fidelity. Hence, these results demonstrate that our approach achieves quality image reconstruction within a reasonable time.

The results of our five-bounce reconstruction approach also reveal that it is more effective in reconstructing point-like objects and long and thin objects (eg. rods), with sharp and clear images. Comparatively, the reconstructed image of the cube-shaped object is slightly blurry due to its complex shape and scattering properties.

6 Discussion

6.1 Generalisation to N-bounce NLOS Imaging

Our method presented in this paper is applicable for generalisation to higher orders of diffuse illumination and bounces. The generalized mathematical expression describing the continuous light transport process is outlined as below,

$$\begin{aligned}\rho^{n+1}(x^{n+1}, y^{n+1}, t^{n+1}, z^{n+1}) = \iiint_{\Omega} \frac{1}{r^3}\rho^n(x^n, y^n, t^n, z^n)\delta((x^{n+1}-x^n)^2 \\ +(y^{n+1}-y^n)^2 + (z^{n+1}-z^n)^2 - (\frac{c(t^{n+1}-t^n)}{2}))dx\,dy\,dz\end{aligned} \tag{23}$$

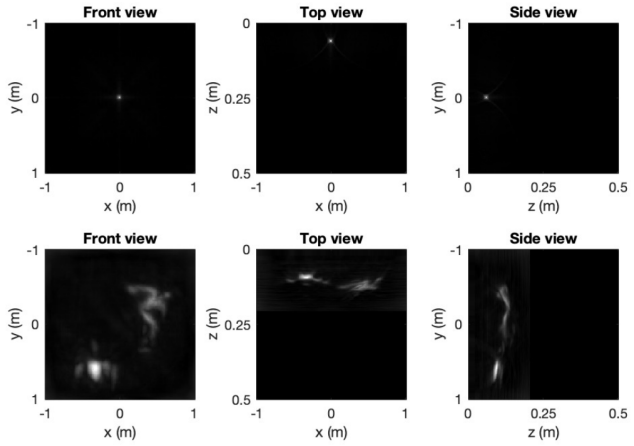

Fig. 5: Reconstruction from A to O: the five-bounce reconstruction for the object. It represents ρ for three scenes, which are the ultimate reconstruction.

Following the above mathematical description, one could derive subsequent discrete models for confocal NLOS imaging in n^{th} order of indirection illumination.

6.2 Limitation

However, there are certain factors that limit the scope of our research. Firstly, the model is constructed solely for confocal scanning and imaging. Conventional imaging has not been proven to work for the algorithm represented. In addition, as the signal strength is relatively weak due to the multi-bounces, our approach requires the use of retroreflective materials on the hidden objects. These two are the main constraints of the five and higher bounce imaging approach's applications. Lastly, the testing is mostly theoretical, and only simulations are used. Future research could also use time-resolved detectors such as the popular SPAD to confirm the results with experiments.

7 Conclusion

Previous NLOS imaging research, including LCT and f-k migration approach, constructs their model on three bounces of diffuse reflections. However, in our research, we investigated what would happen if we break this assumption to be more realistic.

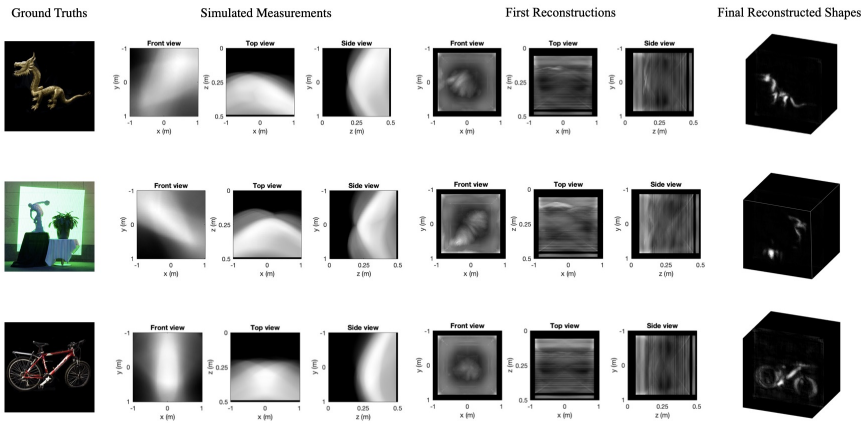

Fig. 6: Simulation Results Overview

We presented a five-bounce NLOS imaging approach with rigorous modeling and transformations. By defining the shift-invariant convolution kernel in the light path and applying fast Fourier transform, we can reconstruct the original object from the measurement with satisfactory computational efficiency. In addition, we tested our model on three different scenes. Our results proved the effectiveness of the five-bounce NLOS approach, and hence paved the foundation for NLOS-Imaging in more complex scenarios in the future.

Despite some potential limitations, our fifth-order NLOS imaging approach is a significant step toward improving the effectiveness and widening the range of applications of NLOS imaging in real-world scenarios. Our research extends the method to deal with higher-order bounces of indirect illuminations in similar problems, and our results suggest that the approach could be extended to other types of scenes and objects. By further addressing the limitations we identified, we believe that our approach would render practical applications in fields such as remote sensing, surveillance, and medical imaging. Overall, we hope that our research will contribute to the development of more advanced and versatile NLOS imaging techniques in the future.

8 Acknowledgement

We are deeply grateful to Professor Feihu Xu, our mentors Likang Zhang and Juntian Ye, and Tencent's Program for Young Scholars in Math and Science for their invaluable support.

Throughout the research, the team had a clear assignment of work. While Ge focused more on literature review, simulation results, and presenting, Xisen was

more in charge of problem layout, mathematical modeling, simulation methodology, and program implementation.

We would like to first extend our heartfelt gratitude to Professor Feihu Xu for his guidance, expertise, and support throughout the research process. His deep knowledge and insights in the area of single-photon imaging and NLOS Imaging were crucial in shaping the direction of our research and ensuring the research's success.

We are also immensely grateful to Tencent's Program for their generous support of our research project. Their resources and support were critical in enabling us to making meaningful contributions to our field of study.

Finally, we wish to express our sincere gratitude to our mentors: Juntian Ye and Likang Zhang. Their guidance and mentorship provided us with crucial support and feedback on our research methodology, data simulation, and presentation of our findings. They also helped us to navigate the challenges and obstacles we encountered during the research, providing us with invaluable support and encouragement. We appreciate their gracious professionalism.

References

1. Arellano, V., Gutierrez, D., & Jarabo, A. (2017). Fast back-projection for non-line of sight reconstruction. ACM SIGGRAPH 2017 Posters. https://doi.org/10.1145/3102163.3102241
2. Baradad, M., Ye, V., Yedidia, A. B., Durand, F., Freeman, W. T., Wornell, G. W., Torralba, A. (2018). Inferring light fields from shadows. 2018 IEEE/CVF Conference on Computer Vision and Pattern Recognition. https://doi.org/10.1109/cvpr.2018.00656
3. Boger-Lombard, J., Katz, O. (2019). Passive optical time-of-flight for non line-of-sight localization. Nature Communications, 10(1). https://doi.org/10.1038/s41467-019-11279-6
4. Bouman, K. L., Ye, V., Yedidia, A. B., Durand, F., Wornell, G. W., Torralba, A., Freeman, W. T. (2017). Turning corners into cameras: Principles and methods. 2017 IEEE International Conference on Computer Vision (ICCV). https://doi.org/10.1109/iccv.2017.249
5. Buttafava, M., Zeman, J., Tosi, A., Eliceiri, K., Velten, A. (2015). Non-line-of-sight imaging using a time-gated single photon avalanche diode. Optics Express, 23(16), 20997. https://doi.org/10.1364/oe.23.020997
6. Gariepy, G., Tonolini, F., Henderson, R., Leach, J., Faccio, D. (2015). Detection and tracking of moving objects hidden from view. Nature Photonics, 10(1), 23–26. https://doi.org/10.1038/nphoton.2015.234
7. Gkioulekas, I., Levin, A., Durand, F., Zickler, T. (2015). Micron-scale light transport decomposition using interferometry. ACM Transactions on Graphics, 34(4), 1–14. https://doi.org/10.1145/2766928
8. Gupta, M., Nayar, S. K., Hullin, M. B., Martin, J. (2015). Phasor imaging. ACM Transactions on Graphics, 34(5), 1–18. https://doi.org/10.1145/2735702
9. Gupta, O., Willwacher, T., Velten, A., Veeraraghavan, A., & Raskar, R. (2012). Reconstruction of hidden 3D shapes using diffuse reflections. Optics Express, 20(17), 19096. https://doi.org/10.1364/oe.20.019096

10. Heide, F., Xiao, L., Heidrich, W., amp; Hullin, M. B. (2014). Diffuse mirrors: 3D reconstruction from diffuse indirect illumination using inexpensive time-of-flight sensors. 2014 IEEE Conference on Computer Vision and Pattern Recognition. https://doi.org/10.1109/cvpr.2014.418
11. Jarabo, A., Masia, B., Marco, J., Gutierrez, D. (2017). Recent advances in transient imaging: A Computer Graphics and vision perspective. Visual Informatics, 1(1), 65–79. https://doi.org/10.1016/j.visinf.2017.01.008
12. Katz, O., Heidmann, P., Fink, M., Gigan, S. (2014). Non-invasive single-shot imaging through scattering layers and around corners via speckle correlations. Nature Photonics, 8(10), 784–790. https://doi.org/10.1038/nphoton.2014.189
13. Kirmani, A., Hutchison, T., Davis, J., amp; Raskar, R. (2009). Looking around the corner using transient imaging. 2009 IEEE 12th International Conference on Computer Vision. https://doi.org/10.1109/iccv.2009.5459160
14. Klein, J., Peters, C., Martín, J., Laurenzis, M., / Hullin, M. B. (2016). Tracking objects outside the line of sight using 2D intensity images. Scientific Reports, 6(1). https://doi.org/10.1038/srep32491
15. Laurenzis, M., & Velten, A. (2014). Feature selection and back-projection algorithms for nonline-of-sight laser–gated viewing. Journal of Electronic Imaging, 23(6), 063003. https://doi.org/10.1117/1.jei.23.6.063003
16. Lindell, D. B., Wetzstein, G., & O'Toole, M. (2019). Wave-based non-line-of-sight imaging using fast F-k migration. ACM Transactions on Graphics, 38(4), 1–13. https://doi.org/10.1145/3306346.3322937
17. Liu, X., Guillén, I., La Manna, M., Nam, J. H., Reza, S. A., Huu Le, T., Jarabo, A., Gutierrez, D., & Velten, A. (2019). Non-line-of-sight imaging using phasor-field virtual wave optics. Nature, 572(7771), 620–623. https://doi.org/10.1038/s41586-019-1461-3
18. O'Toole, M., Heide, F., Lindell, D. B., Zang, K., Diamond, S., Wetzstein, G. (2017). Reconstructing transient images from single-photon sensors. 2017 IEEE Conference on Computer Vision and Pattern Recognition (CVPR). https://doi.org/10.1109/cvpr.2017.246
19. O'Toole, M., Lindell, D. B., & Wetzstein, G. (2018). Confocal non-line-of-sight imaging based on the light-cone transform. Nature, 555(7696), 338–341. https://doi.org/10.1038/nature25489
20. Pediredla, A. K., Buttafava, M., Tosi, A., Cossairt, O., amp; Veeraraghavan, A. (2017). Reconstructing rooms using Photon echoes: A plane based model and reconstruction algorithm for looking around the corner. 2017 IEEE International Conference on Computational Photography (ICCP). https://doi.org/10.1109/iccphot.2017.7951478
21. Saunders, C., Murray-Bruce, J., Goyal, V. K. (2019). Computational periscopy with an ordinary digital camera. Nature, 565(7740), 472–475. https://doi.org/10.1038/s41586-018-0868-6
22. Shin, D., Xu, F., Venkatraman, D., Lussana, R., Villa, F., Zappa, F., Goyal, V. K., Wong, F. N., Shapiro, J. H. (2016). Photon-efficient imaging with a single-photon camera. Nature Communications, 7(1). https://doi.org/10.1038/ncomms12046
23. Sun, B., Edgar, M. P., Bowman, R., Vittert, L. E., Welsh, S., Bowman, A., Padgett, M. J. (2013). 3D computational imaging with single-pixel detectors. Science, 340(6134), 844–847. https://doi.org/10.1126/science.1234454
24. Wang, J., Liu, S., Meng, X., Gao, W., amp; Yuan, J. (2021). Application of retroreflective materials in urban buildings: A comprehensive review. Energy and Buildings, 247, 111137. https://doi.org/10.1016/j.enbuild.2021.111137

25. Velten, A., Wu, D., Jarabo, A., Masia, B., Barsi, C., Joshi, C., Lawson, E., Bawendi, M., Gutierrez, D., Raskar, R. (2013). Femto-photography. ACM Transactions on Graphics, 32(4), 1–8. https://doi.org/10.1145/2461912.2461928
26. Xu, F., Shulkind, G., Thrampoulidis, C., Shapiro, J. H., Torralba, A., Wong, F. N., & Wornell, G. W. (2018). Revealing hidden scenes by photon-efficient occlusion-based opportunistic active imaging. Optics Express, 26(8), 9945. https://doi.org/10.1364/oe.26.009945